Thermal Denaturation of Hydrated Wool Keratin by ^{1}H Solid-State NMR

Maria Baias,*,‡ Dan E. Demco,*,†,§ Crisan Popescu,*,†,|| Radu Fechete,§ Claudiu Melian,† Bernhard Blümich,‡ and Martin Möller†

DWI an der RWTH-Aachen University, Pauwelsstrasse 8, D-52056 Aachen, Germany, Institut für Technische and Makromolekulare Chemie, RWTH Aachen University, Worringer Weg 1, D-52074 Aachen, Germany, Department of Physics, Technical University Cluj-Napoca, RO-400020 Cluj-Napoca, Romania, and University "Aurel Vlaicu" Arad, Bd. Revolutiei 77, RO-310130 Arad, Romania

Received: October 25, 2008; Revised Manuscript Received: December 11, 2008

Thermal denaturation of hydrated keratin in wool was investigated by NMR using ^{1}H wide-line spectra to obtain the phase composition and ^{1}H spin-diffusion experiments using a double-quantum filter to obtain the domain sizes for the wool fibers. The denaturation process detected by DSC takes place for wool fibers in deuterated water in the temperature range 140−144 °C. The phase composition measured by ^{1}H wide line NMR spectra reveals a rigid, semirigid and an amorphous phase for temperatures in the range 25−160 °C. A dramatic change in the phase composition was detected around 142 °C, corresponding to the denaturation temperature. The morphological domain sizes measured by ^{1}H spin-diffusion NMR experiments were obtain from the solutions of the spin-diffusion equations for two-dimensional rectangular and cylindrical morphologies. The keratin mobility gradient in the interfacial region at different denaturation temperatures was measured from the ^{1}H spin-diffusion data. A qualitative model describing the denaturation process of hydrated keratin protein was developed that explains the changes in domain thickness, spin diffusivities, phase composition, and thermodynamic parameters.

1. Introduction

Proteins exhibit their active properties within certain temperature ranges and unfold beyond the limits. The intervals are around room temperature, although for many industrial applications of enzymes it would be of interest to have them active at higher values of temperature. A few proteins withstand temperatures above 100 °C and among them there are some of the fibrous proteins.

Fibrous proteins are distinguished from globular proteins by their filamentous, elongated form. Most of them play structural roles in animal cells and tissues. Among the most notorious representatives of this class are the α-keratins in human hair, wool. and finger nails, fibroin in silk, Actin and myosin in muscles, and collagen, the most abundant protein in vertebrate bodies.

The model describing keratin fibers is that of a crystalline rodlike α-helix (intermediate filaments, IFs) embedded in an amorphous matrix (Figure 1), (intermediate filament associated proteins, IFAP) having a relatively high amount of cystine.[1] Although the model was proposed for describing the mechanic behavior of keratins, it appeared to be also suitable for explaining the high denaturation temperature found at keratins.[2,3] In soluble proteins the helix denaturates (unfolds) at temperatures up to 80 °C. There are no data on the denaturation temperature of IFs alone (not surrounded by a matrix) but one may expect that α-helix from keratins would also unfold at temperatures around 80 °C. The fact that keratin proteins show the denaturation at above 200 °C is assumed to be due to the rigidity of the matrix, whose viscosity impedes the unfolding of the helix. The viscosity (and cross-link) of the matrix governs, therefore, the segmental mobility of the α-helix and the unfolding reaction (denaturation).

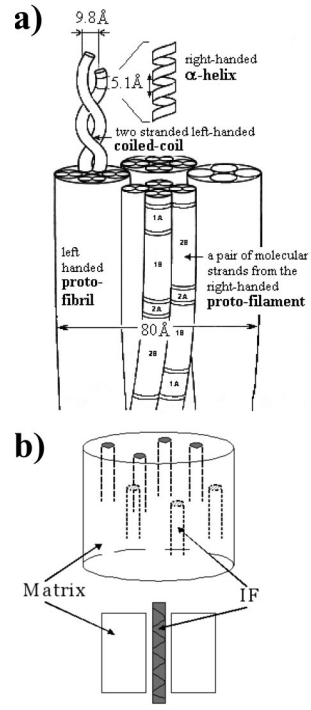

Figure 1. (a) The intermediate filament structure; (b) schematic representation of the two-phase model of keratin fibers. The intermediate filaments (IF) are imbedded in an amorphous keratin matrix.

* To whom correspondence should be addressed. E-mail: mbaias@mc.rwth-aachen.de, popescu@dwi.rwth-aachen.de, demco@mc.rwth-aachen.de. Fax: +49-241-233-01.

‡ Institut für Technische and Makromolekulare Chemie, RWTH Aachen University.

† DWI an der RWTH-Aachen University.

§ Technical University Cluj-Napoca.

|| University "Aurel Vlaicu" Arad.

10.1021/jp8094616 CCC: $40.75
Published on Web 01/27/2009

A similar model was proposed for collagen based materials.[4] The model suggests that added solvents able to decrease the viscosity of the matrix depress the temperature of unfolding. This has been indeed noticed in DSC experiments with keratin fibers[5,6] and with collagen based materials (parchments, leathers) in water environment.[7−9]

Understanding properly how the keratins protect the intermediate filaments against thermal denaturation until high values of temperature is of a clear interest for the fundamental knowledge of protein denaturation. The role of matrix in this process may suggest ways for designing high-temperature stable proteins as new biomaterials.

Multinuclear and multidimensional liquid- and solid-state NMR are important techniques in structural biology.[10−12] They are well suited to the investigation of noncrystalline molecules, such as proteins, that are almost impossible to study using other experimental techniques. Recently, a ^{13}C and ^{2}H solid-state NMR study of an α-keratin sourced from equine hoof has revealed a strong dependence of molecular conformation and molecular dynamics on the degree of hydration of the material.[13] In particular, dehydration results in a much more rigid and ordered structure, with a loss of α-helical components in the structure and breaking of cysteine disulfide linkages. Moreover, the molecular dynamics and structural organization of mouse epidermal keratin intermediate filaments (IF) have been studied via ^{13}C and ^{2}H spectroscopy and relaxometry on IF labeled with isotopically enriched amino acids.[14] Solid-state ^{31}P NMR spectroscopy was also applied to the analysis of phosphorylated wool keratin to investigate the modification located on the surface of wool keratin.[15]

The clarification of the fine structure of fibrous proteins that include keratin in the solid state is very important for the understanding of their nature. This is based on the fact that ^{13}C and ^{15}N chemical shifts of polypeptides are substantially dependent on their main-chain conformations such as α-helix and β-sheet forms. Using this method it was confirmed that both right-handed α-helix and β-sheet forms exist in native wool fiber.[16,17]

Spin-diffusion NMR was proved to be a useful method for characterization of semicrystalline polymer morphology.[18−22] The sizes of the rigid, interfacial, and amorphous fractions can be estimated from such experiments and the results compared well to that from TEM and X-ray diffraction. To the best of our knowledge no spin-diffusion experiments were reported on keratin.

The aim of this work is to investigate the effect of thermal denaturation of hydrated wool keratin by ^{1}H NMR wide-line spectroscopy and ^{1}H spin diffusion. The phase (fraction) composition will be measured from ^{1}H wide-line spectra *ex situ* for different denaturation temperatures. Three fractions are detected, that is, rigid, interfacial, and amorphous. The domain sizes for different stages of denaturation were measured by ^{1}H spin-diffusion using two different wool keratin morphologies. The molecular dynamics of the interfacial region can be investigated using the ^{1}H spin-diffusion NMR experiments. The changes in the degree of keratin organization, the amount of different phases and molecular dynamics are discussed in correlation with the temperatures during the thermal denaturation process.

2. Experimental Details

2.1. Samples. Keratin fibers from 23 μm diameter wool were used for the current investigation. The samples were cut into fine snippets (~2 mm), for easy handling. The reference sample was swelled in $^{2}H_2O$ for one week. The parts of the swollen wool fibers were introduced in stainless steel capsules and treated at different temperatures in a DSC instrument (see below). The denaturation process was followed at different temperatures until +160 °C. The NMR samples were gathered from deuterium oxide-DSC experiments, taking the capsules at various moments linked to thermal events as disclosed by DSC. Five samples were prepared at the temperatures of 25, 134, 142, 149, and 160 °C on which NMR measurements were made.

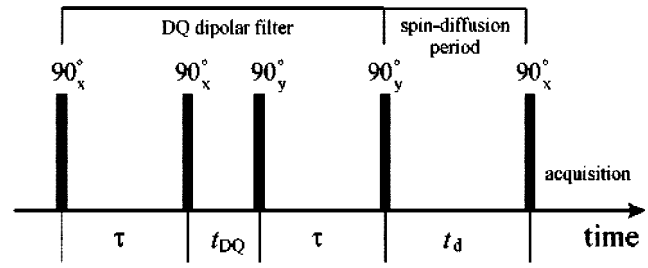

Figure 2. Scheme for the spin-diffusion experiment with a DQ filter. The first two pulses excite DQ coherences that evolve for a short time t_{DQ}. These coherences are converted by the following two pulses into z-magnetization. The spin diffusion takes place during the time interval of duration t_d. The last pulse read out the distribution of magnetization between different keratin phases.

2.2. Proton and ^{13}C NMR Measurements. Proton solid-state NMR spectra, ^{1}H double-quantum (DQ) build-up curves, ^{1}H spin-diffusion, and ^{13}C CPMAS spectra were measured on a Bruker DSX-500 spectrometer operating at 500.45 MHz, and 125.84 MHz for ^{1}H and ^{13}C, respectively. Proton NMR data were collected at room temperature for nonspinning samples. The dead time of the spectrometer is 5.5 μs. The length of a $\pi/2$ pulse was about 5.5 μs, the dwell time was 2 μs, and the recycle delay was 3 s for all measurements.

Proton spin-diffusion measurements were performed using the general scheme consisting of a double-quantum (DQ) dipolar filter, a spin-diffusion period, and an acquisition period as presented in Figure 2. The gradient of magnetization was created by the dipolar filter that excites DQ coherences (Figure 2) and selects mainly the magnetization of the rigid phase (fraction).[21,22] The pulse sequence is based on the two pulses acting during the excitation and reconversion periods. The value of the excitation/reconversion times used in the spin-diffusion experiments is $\tau = 7$ μs. It corresponds to the rising region of the DQ build-up curve for each sample (see below).

The experimental wide-line spectra were decomposed in three components using the DMFIT program. The broad component describing the rigid fraction of the spectra was approximated by a Gaussian function. A Lorentzian line shape was used to describe the narrow component of the spectra corresponding to the mobile phase. A combination of Gaussian and Lorenzian functions was used to describe the intermediate line corresponding to the interface.

The proton NMR DQ build-up curves were recorded for setting the optimum parameters of the DQ dipolar filter. They were measured on a Bruker DSX-500 spectrometer at a proton resonance frequency of 500.45 MHz. The duration of the applied 90° pulses was 5.5 μs. The DQ evolution time and the z-filter delay were fixed to $t_{DQ} = t_d = 5$ μs (Figure 2).

^{13}C NMR spectra were measured using the cross-polarization (CP) magic-angle sample spinning (MAS) with power decoupling by two-pulse phase modulation (TPPM) method. The contact pulse for CP has a duration of 3 ms.

2.3. Differential Scanning Calorimetry (DSC). The DSC investigations were performed on a DSC 7 Perkin Elemer, using

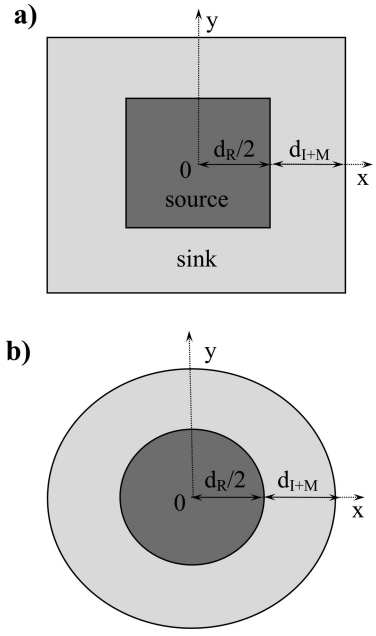

Figure 3. Schematic representation of the rectangular (a) and cylindrical (b) morphologies used to approximate the keratin tertiary structure. The size of interface and mobile (amorphous) fractions is doted by d_{I+M}, and d_R is the size of the rigid domain.

pressure resistant (25 bar) stainless steel large volume capsules (Perkin Elmer). The temperature ranged from 50 to 180 °C with a heating rate of 10 K/min, while flushing the chamber with nitrogen flow of 10 mL/min. DSC calibration was done with indium and palmitic acid, both of high purity.

Differential scanning calorimetry experiments were carried out, using deuterated water as an environment for keratin during heating. For deuterium oxide−DSC experiments 5−6 mg of snippets were weighed and then transferred in 1 mL deuterium oxide (99.9%) and kept overnight to allow moisture replacement. The sample was then placed in the stainless steel crucible which was sealed with the silicon rubber O-ring, and the peak and enthalpy of the endothermal process was recorded. A minimum of three samples was measured for ensuring the reproducibility of the DSC data.

3. Theory of NMR spin-diffusion

3.1. Spin-Diffusion Observables. The transport of z-magnetization oriented along the static magnetic field in a NMR experiment can be described by the diffusion equation in the continuum approximation. The concentration $m(\vec{r},t)$ of nuclear z-magnetization at position $\vec{r}$ in the sample from the center of symmetry of different morphologies (Figure 3a and b) at the moment of time t is defined by

$$m(\vec{r},t) = \frac{M_z(\vec{r},t)}{\rho(\vec{r})\Delta V(\vec{r})} \tag{1}$$

where $M_z(\vec{r},t)$ is the total z-magnetization and $\Delta V(\vec{r})$ is the infinitesimal volume around the point defined by the vector $\vec{r}$. The number density of spins is denoted by $\rho(\vec{r})$.

In the limit of isotropic spin-diffusion and spatially constant spin diffusivity the spin diffusion equation has the form

$$\frac{\partial m(\vec{r},t)}{\partial t} = D\nabla^2 m(\vec{r},t) \tag{2}$$

The instantaneous NMR observables in a spin-diffusion experiment are represented by the normalized integral intensity $I_i(t)/I_0$ of the ith component of the NMR spectrum with the total integral intensity I_0. More specific the NMR spin-diffusion observables are defined by

$$\frac{I_i(t)}{I_0} = \frac{\oint\oint\oint_{V_i} \rho_i m_i(\vec{r},t)d\vec{r}}{I_0} \tag{3}$$

where V_i is the volume of the ith domain.

3.2. Solution of the Spin-Diffusion Equations for a Rectangular Morphology. The real morphology of keratin in wool can be approximated by a square transverse morphology (Figure 3a). We assume that the spin-diffusion takes place in a heterogeneous matrix from a source R with low segmental mobility into a finite sink M with larger segmental mobility. The interfacial region is taken together with the amorphous fraction in the following considerations. The relationships describing the time evolution of the integral intensities of the NMR signals $I_R(t)$ and $I_M(t)$ for a spin-diffusion process of dimensionality $n = 2$ can be obtained from refs 23 and 24. The spin magnetization in the source region (R) for a two-dimensional spin-diffusion process is given by

$$I_R(t) \approx \rho_R[2\int_0^{d_R/2} m_R(x,t)\,dx]^2 \tag{4}$$

where ρ_R is the number density of spins of the source R of size d_R and $m_R(x,t)$ is the space and time dependent concentration of the z spin magnetization. For a dipolar filter that selects only the magnetization of the R region, the spin magnetization in the sink region can be written as

$$I_M(t) = I_R(0) - I_R(t) \tag{5}$$

The quantity $m_R(x,t)$ is given by[23,24]

$$m_R(x,t) = \frac{\rho_R d_R m_{0R}}{\rho_R d_R + \rho_M d_M} - \sum_{m=1}^{\infty} 2m_{0R}\sin[kd_M\beta_m]\cos[x\beta_m]\exp[-D_R\beta_m^2 t]\beta_m^{-1} \times \{[\sigma d_R + kd_M]\cos[d_R\beta_m]\cos[kd_M\beta_m] - [\sigma k d_M + d_R]\sin[d_R\beta_m]\sin[kd_M\beta_m]\}^{-1} \tag{6}$$

where d_M is the size of the sink ($d_M \approx d_{I+M}$), ρ_M is the number density of spins in the region M, $k = (D_R/D_M)^{1/2}$, and $\sigma = k\rho_R/\rho_M$. The spin-diffusion coefficients in the regions R and M are denoted by D_R and D_M, respectively. The quantities β_m, (m = 1, 2, 3,...) are the roots of a trigonometric equation[23,24]

$$\rho_R k\sin(d_R\beta)\cos(kd_M\beta) + \rho_M\cos(d_R\beta)\sin(kd_M\beta) = 0 \tag{7}$$

We shall note that the ratio d_M/d_R can be evaluated from the thermal equilibrium values of the R and M spectral components, that is,

$$E = \frac{I_{M,eq}}{I_{R,eq}} = \frac{\rho_M V_M}{\rho_R V_R} \quad (8)$$

where V_M and V_R are the volumes of the domains. For the square morphology (Figure 3a) we can finally write

$$\frac{d_M}{d_R} = \frac{1}{2}\left[\left(E\frac{\rho_R}{\rho_M} + 1\right)^{1/2} - 1\right] \quad (9)$$

The above equation can be used for reducing the number of independent parameters for the decay and buildup curves of spin diffusion.

3.3. Spin-Diffusion for a Cylindrical Morphology. We shall consider in the following a more realistic morphology for the spin-diffusion in wool keratin that is represented by cylindrical morphology (cf. Figure 3b). The rigid domains selected by a double-quantum dipolar filter are represented by the intermediate filaments (Figure 1) that are surrounded by the amorphous keratin region. For simplicity we consider mobile (amorphous) and interface regions as the sink for the ^{1}H magnetization.

For a cylindrical morphology the spin-diffusion equation for the instantaneous concentration of z-magnetization $m(r,t)$ at distance r from the center of cylinder is given by[25]

$$\frac{\partial m(r,t)}{\partial t} = \frac{1}{r}\frac{\partial}{\partial r}\left[rD\frac{\partial m(r,t)}{\partial r}\right] \quad (10)$$

For a constant spin diffusivity D the above equation can be written as

$$\frac{\partial m(r,t)}{\partial t} = \frac{D}{r}\frac{\partial m(r,t)}{\partial r} + D\frac{\partial^2 m(r,t)}{\partial r^2} \quad (11)$$

The equations of spin diffusion in a two-phase composite medium R and M (Figure 3b) have the following forms:

$$\frac{\partial m_R(r,t)}{\partial t} = \frac{D_R}{r}\frac{\partial m_R(r,t)}{\partial r} + D_R\frac{\partial^2 m_R(r,t)}{\partial r^2};(0 \le r \le d_R/2), \quad (12)$$

and

$$\frac{\partial m_M(r,t)}{\partial t} = \frac{D_M}{r}\frac{\partial m_M(r,t)}{\partial r} + D_M\frac{\partial^2 m_M(r,t)}{\partial r^2}; \quad (d_R/2 \le r \le (d_M + d_R)/2) \quad (13)$$

The solutions of the above equations have to be obtained using the initial and boundary conditions. Considering an ideal magnetization filter we can write,

$$m_R(r,t)|_{t=0} = m_{0R} \quad (14)$$

$$m_M(r,t)|_{t=0} = 0 \quad (15)$$

where the magnetization concentration at the end of dipolar filter action is m_{0R}. Two boundary conditions need to be also specified. The first boundary condition is related to the continuity of the z-magnetization concentration at the domain boundary, that is, for $r = d_R/2$, we have

$$m_R(r,t)|_{r=d_R/2} = m_M(r,t)|_{r=d_R/2} \quad (16)$$

The second boundary condition corresponds to the fact that magnetization fluxes, defined by the relation $j(\vec{r},t) = -D\rho\nabla\cdot m(\vec{r},t)$, have to be equal at the domain interface. The following relation can be written

$$\rho_R D_R\frac{\partial}{\partial r}m_R(r,t)|_{r=d_R/2} = \rho_M D_M\frac{\partial}{\partial r}m_M(r,t)|_{r=d_R/2} \quad (17)$$

The NMR spin-diffusion observables for the cylindrical morphology are defined by the relationships

$$\frac{I_R(t)}{I_0} = \frac{\int_0^{d_R/2} r m_R(r,t)\,dr}{I_0} \quad (18)$$

and

$$\frac{I_M(t)}{I_0} = \frac{\int_{d_R/2}^{(d_M+d_R)/2} r m_M(r,t)\,dr}{I_0} \quad (19)$$

In the time regime in which the spin diffusion is not affected by the spin−lattice relaxation, the theorem of total magnetization conservation leads to

$$\frac{I_R(t)}{I_0} + \frac{I_M(t)}{I_0} = 1 \quad (20)$$

which shows that in this case the two NMR observables are not independent.

For a spin system in thermodynamic equilibrium with a thermal bath we can define the ratio E between the total z-magnetization in the M and R domains given by eq 18 and 19. The volume of the cylindrical domains can be easily evaluated and from eq 20 we can finally write

$$\frac{d_M}{d_R} = \frac{1}{2}\left[\left(E\frac{\rho_R}{\rho_M} + 1\right)^{1/2} - 1\right] \quad (21)$$

Equation 21 established a relationship between the domain sizes independent of the spin-diffusion data.

Analytical solutions for the spin-diffusion equations can be established only for a composite medium with a uniform value of spin diffusivities.[20] Realistic values for the domain sizes for a heterogeneous medium with spin-diffusivities $D_R \neq D_M$ can be obtained by the numerical solutions of eq 12 and 13 with supplementary conditions eq 14−17, and 21.

4. Results and Discussion

4.1. Thermal Denaturation by DSC. A typical DSC plot of keratin (wool) fiber in deuterated water is shown in Figure 4. The endothermal process recorded around 140 °C is attributed to the thermal denaturation of keratin by melting of the α-helix

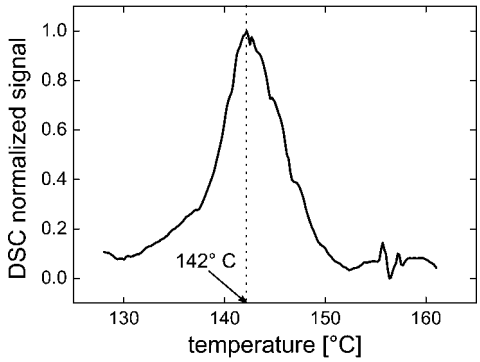

Figure 4. DSC normalized signal of a wool sample in D_2O for the temperature range of denaturation.

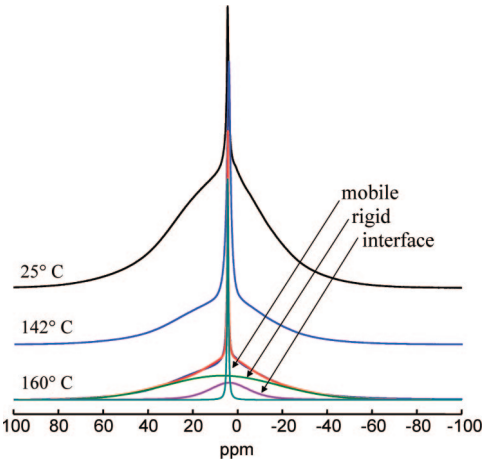

Figure 5. Proton NMR spectra of native (25 °C) and denaturated wool keratin fibers at temperatures 142 and 160 °C. All spectra were decomposed into three components corresponding to the rigid, semirigid (interface), and mobile fractions.

crystalline structure.[26] The peak is quite different from a DSC in water environment, where the endothermal process appears as a doublet (peaks around 138 and 144 °C), attributed to the denaturation of α-helix in ortho and para cells which form wool cortex.[27] This difference between the experiments in water and deuterated water suggests that hydrogen bonds play a significant role in the thermal denaturation process of wool and supports the model of interface scaffolding the crystalline part which was recently proposed for keratin fibers.[28] The scenario for the thermal denaturation of hydrated keratin as reflected in the DSC and NMR data will be discussed below.

4.2. Proton NMR Spectra and Phase Composition. Proton NMR spectra of hydrated wool keratin samples denaturated at different temperatures, recorded in static conditions, are presented in Figure 5. The best fitting parameters have been found by decomposing the spectra in three lines described by a Gaussian, a Lorenzian, and a combination of Gaussian and Lorenzian functions, respectively. The broad component, associated with the Gaussian line, corresponds to the rigid phase. The Lorenzian line associated with the narrow component of the spectra describes the mobile phase. The intermediate line, described by the combination of Gaussian and Lorenzian functions is associated with the interface.

The phase composition of the investigated hydrated wool keratin samples is shown in Figure 6 as a function of denaturation temperature. The measurements reveal an increased amount of mobile phase at the expense of the rigid phase in the temperature region where the denaturation process occurs. The phase (fraction) composition at temperatures higher than

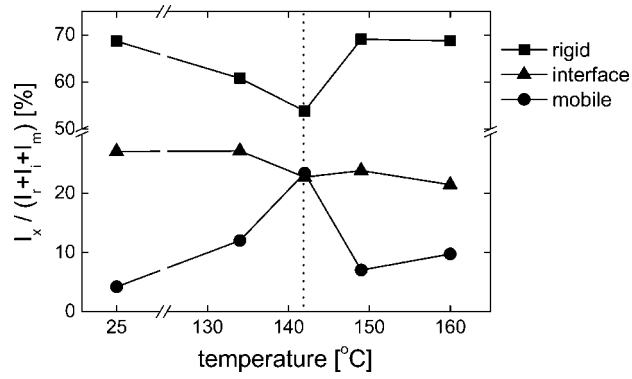

Figure 6. The phase (fraction) composition of hydrated keratin wool fibers at different denaturation temperatures.

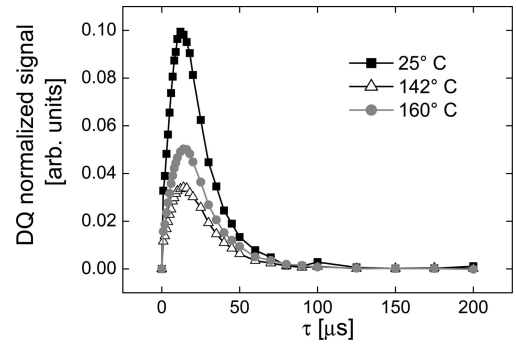

Figure 7. Normalized ^{1}H DQ signals for native and denaturated wool keratin samples at different denaturation temperatures.

142 °C are similar (but not identical) with those measured around the ambient temperature.

4.3. Double-Quantum Dipolar Filter for ^{1}H Spin Diffusion. The spin-diffusion experiments observe the equilibration of spatially heterogeneous magnetization over the sample. A gradient in the magnetization can be created, for example, with a dipolar filter which excites double-quantum (DQ) coherences.[24] This type of filter is more advantageous than a dipolar filter for mobile domains because it allows a more accurate detection of the narrow signals on the top of the broad component as compared to the detection of a broad component under a narrow signal. This is valid especially at short diffusion times when the magnetization of one of the components is very small.

The DQ filter can be set such to select the magnetization only from the most rigid part of a heterogeneous sample. By choosing appropriate excitation/reconversion periods τ (Figure 2) of the double-quantum coherences, the magnetization corresponding to the stronger dipolar couplings will pass through the filter and that of the weaker dipolar couplings is filtered out. The optimum value of τ can be chosen by recording DQ build-up curves as shown in Figure 7 for the nondenaturated (25 °C) and denaturated (160 °C) wool samples. The DQ build-up curves were recorded using a five-pulse sequence with a spin-diffusion time of $t_d = 5$ μs (Figure 2). The maxima of the DQ build-up curves appear at very short excitation/reconversion times τ of about 10−12 μs for all investigated wool samples. In this range of τ values, the mobile component is completely filtered out as shown below. This shows that ^{1}H dipolar couplings are larger for the native sample compared with the sample denaturated at 160 °C. The slope of the DQ build-up curves in the initial regime of the excitation/reconversion times is related to the residual van Vleck second moment of the rigid fraction.[10] Figure 7 shows that the residual dipolar interactions change to some extent during the denaturation process. The

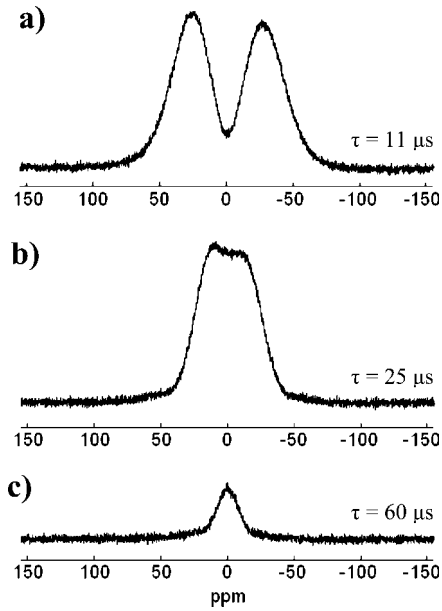

Figure 8. Proton DQ filtered NMR spectra recorded for different values of the excitation/reconversion time (a) $\tau = 11$ μs, (b) $\tau = 25$ μs, and (c) $\tau = 60$ μs (Figure 2).

TABLE 1: Proton Second van Vleck Moments for Native and Thermally Denaturated Hydrated Keratin Fibers

T (°C)	$\langle M_2 \rangle$ (10^9 Hz^2)
25	5.96
142	2.14
160	2.7

maximum of the DQ build-up curve of the native sample is slightly shifted to smaller τ values compared to the denaturated samples. This indicates that ^{1}H dipolar couplings are larger for the native sample compared with the sample denaturated at 142 °C. The proton−proton average distances inside the collapsed intermediate filaments become larger compared to the native sample.

The DQ-filtered NMR spectra recorded for different values of the excitation/reconversion times τ are shown in Figure 8 for the nondenaturated sample. For short τ values the DQ filtered ^{1}H spectrum edits mainly the spin-pairs with the strongest dipolar couplings (Figure 8a). In the region of the maximum of the DQ build-up curves the pulse sequence edits a dipolar network of many spins corresponding to the crystalline and partially the interface fraction (Figure 8b). The ^{1}H spectrum in Figure 8c filtered only the keratin from the amorphous fraction. The value of $\tau = 5$ μs has been chosen for the dipolar filter of the rigid domain, which still keeps the filter efficiency close to unity with a reasonable value of the signal−to−noise ratio.

4.4. Proton Residual Second van Vleck Moments. The measurements of the residual second van Vleck moment using DQ build-up curves (Figure 7) were reported in ref 21, and the resultant values are summarized in Table 1. Similar to the spin diffusivities, the second van Vleck moment $\langle M_2 \rangle$ has the lowest value for the denaturated keratin fibers which were heated at the denaturation temperature, showing a decrease in strength of the dipole−dipole interaction, in connection with the loss of rigidity in the temperature range of the denaturation process.

4.5. Proton Spin Diffusivities. An accurate analysis of the thickness of domains by NMR spin-diffusion experiments requires three steps. These are (i) an optimization of a dipolar filter to obtain the highest selectivity to the different phases (see section 4.3), (ii) knowledge of the spin-diffusion coefficients

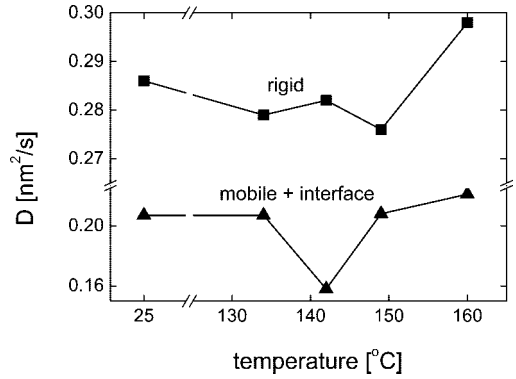

Figure 9. Effective ^{1}H spin-diffusivities evaluated from eq 22 and eq 23 for the phases of wool keratin as a function of the denaturation temperature.

for modeling the experimental data, and (iii) proper choice of a model that describes the morphology of the material studied (this section). The spin-diffusion coefficients can be expressed in terms of the local dipolar field, so that the spin diffusivities are related to the second van Vleck moments.

The values of the spin-diffusion coefficients $D_{R,}$ and D_M for the rigid and soft fractions, respectively, can be determined by approximating the NMR line shapes of the rigid and the soft fractions by Gaussian and Lorentzian functions, respectively. The spin-diffusion coefficients can be related to the second van Vleck moment of the NMR absorption lines, which, in turn, are related to the full line width $\Delta\nu_{1/2}$ at half-height.

The equations describing the spin-diffusion coefficients for rigid (Gaussian line) and mobile (Lorentzian line) regions are given by,[20]

$$D_R = \frac{1}{12}\sqrt{\frac{\pi}{2\ln 2}}\langle r^2\rangle \Delta\nu_{1/2} \tag{22}$$

and

$$D_M = \frac{1}{6}\langle r^2\rangle [\alpha\Delta\nu_{1/2}]^{1/2} \tag{23}$$

where α is the cutoff parameter of the Lorentzian line, $\Delta\nu_{1/2}$ is the full line width at half-height, and $\langle r^2\rangle$ is the mean square distance between the nearest spins. An estimation of $\langle r^2\rangle^{1/2} \approx 0.22$ nm was given for wool keratin, taking into account the amino acid composition.[13]

The calculated spin-diffusion coefficients using eq 22 and 23 are shown in Figure 9. The values of the spin-diffusion coefficient for the region composed of the mobile and interface fractions decrease in the temperature range where the denaturation process occurs. That can be interpreted as disordered keratin fibrils with larger interproton distances. A reorganization that increases the degree of packing will lead at higher denaturation temperatures to larger values of spin diffusivitiy.

4.6. Morphology and Domain Sizes. The spin-diffusion experiments were performed on keratin fibers after they were heated at the following temperatures: 25, 134, 142, 149, and 160 °C. Proton wide-line NMR spectra recorded at three different diffusion times t_d are shown in Figure 10. In all cases the flow of magnetization from the rigid domain into the mobile domain is observed with increasing diffusion times. At short diffusion times mainly the rigid fraction of keratin composed of the α-helical conformation of the intermediate filament is

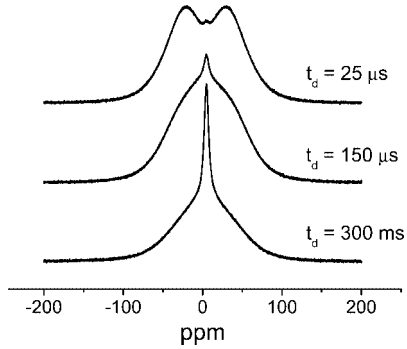

Figure 10. Proton wide-line NMR spectra recorded at three different spin-diffusion times t_d after the action of the DQ dipolar filter (Figure 2).

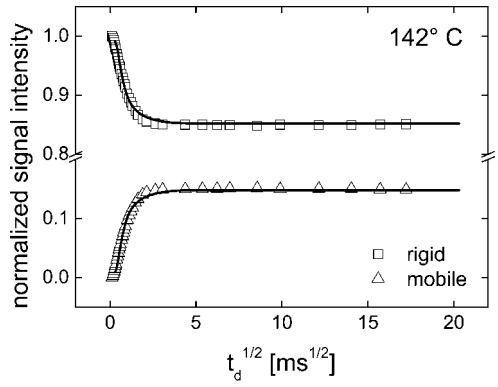

Figure 11. The normalized signal intensities for ^{1}H spin-diffusion experiment (Figure 2) for a wool fiber denaturated at 142 °C.

observed, and can be seen in Figure 10 for $t_d = 25$ μs. Upon increasing the spin-diffusion time, the relative intensity of the rigid fraction in the spectra decreases, and the intensity of the narrow line that originates from the soft amorphous fraction represented by the keratin matrix surrounding the intermediate filament increases.

The presence of the mobile amorphous regions complicates the interpretation of the spin diffusion data. Because it is less than 10% for all samples and because the flow of magnetization is reaching it only after longer spin-diffusion times, our approach will mainly focus on the transfer of magnetization between the crystalline and the less-mobile amorphous regions. Therefore, a renormalization of the integral intensities corresponding to these two phases was made by adding the signal of the amorphous phase to the signal of the interface. The time evolution of the nuclear magnetization for native and denaturated samples with increasing spin-diffusion time is shown in Figure 11 for the rigid and less rigid fraction of the keratin fibers. The quasi-equilibrium is reached after about 4 ms.

To estimate the domain sizes for the rigid and less-mobile amorphous domains based on the analysis of spin-diffusion data, two different cases of morphology were analyzed: Two-dimensional (2D) square morphology and 2D cylindrical morphology as discussed in sections 3.2 and 3.3. Using ^{1}H spin diffusivity shown in Figure 9 the domain sizes of hydrated keratin for different denaturation temperatures are presented in Figure 12. Both morphologies used for domain thickness evaluation leads to similar results in the limit of experimental errors. The rigid domain size increases at the denaturation temperature of 142 °C and mobile and interface thickness decreases. These findings are in agreement with the thermal denaturation scenario discussed below.

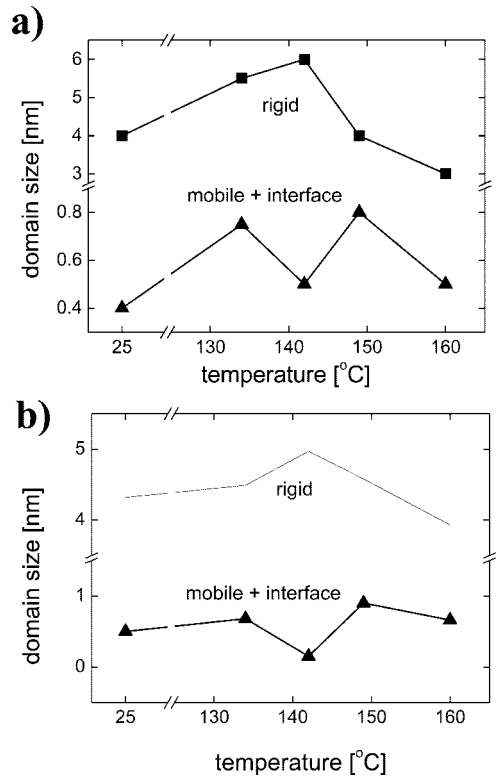

Figure 12. Domain sizes for rigid and mobile + interface fractions of wool keratin as a function of denaturation temperature. The solutions for the spin-diffusion equations for rectangular (a) and cylindrical (b) morphology were used for the evaluation of domain sizes.

4.7. Dynamic Heterogeneity of Hydrated Keratin Fiber Interface. The ^{1}H spin-diffusion experiment using a DQ filter was made on the wool fibers denaturated at different temperatures. The evolution of the z-magnetization front can be measured from the spectral component decomposition. At the beginning of the spin-diffusion experiment the magnetization is stored only in the rigid domain. For short spin-diffusion times the magnetization is present only in the interface and at the longer diffusion times it reaches the mobile region. The average distance $\langle z^2\rangle^{1/2}$ traveled by the ^{1}H z-magnetization can be estimated using an *ad hoc* Einstein relationship in one dimension, that is,

$$\langle z^2\rangle^{1/2} = k\sqrt{2\left(\frac{D_R + D_M}{2}\right)t_d} \qquad (24)$$

where $(D_R + D_M)/(2)$ is the average spin diffusivity, t_d is the spin-diffusion time, and k is an empirical scaling coefficient. The value of this coefficient can be obtained from the thickness of the interface plus mobile domains as measured from spin-diffusion experiments (see Figure 12). To this purpose the relationship $d_M \approx k(2D_M t_{d,max})^{1/2}$ was used where $t_{d,max}$ is the spin-diffusion time where the mobile domain magnetization reaches the quasi-equilibrium.

The interfacial region has a gradient in molecular mobility and therefore a monotonic change in the line-width at the half-intensity can be detected. At smaller spin-diffusion times the experiment edits the part of the interface closer to rigid region and at the longer diffusion times the most mobile part of the interface connected to the mobile region. The gradual changes in the line-width at the half-intensity of the interface spectral component is shown in Figure 13. A gradual change in $\Delta\nu_{1/2}$ is

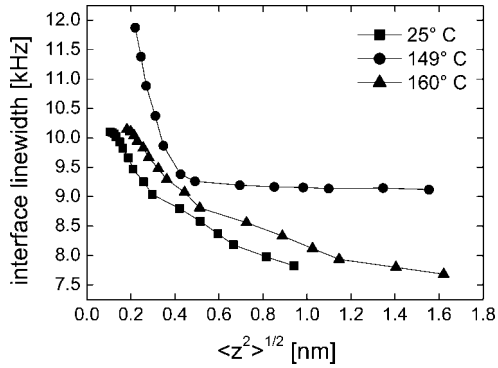

Figure 13. Full line-width at the half-intensity of the interfacial component of the ^{1}H NMR spectrum for wool fibers as a function of spin-diffusion average distance $\langle z^2\rangle^{1/2}$ for different denaturation temperatures.

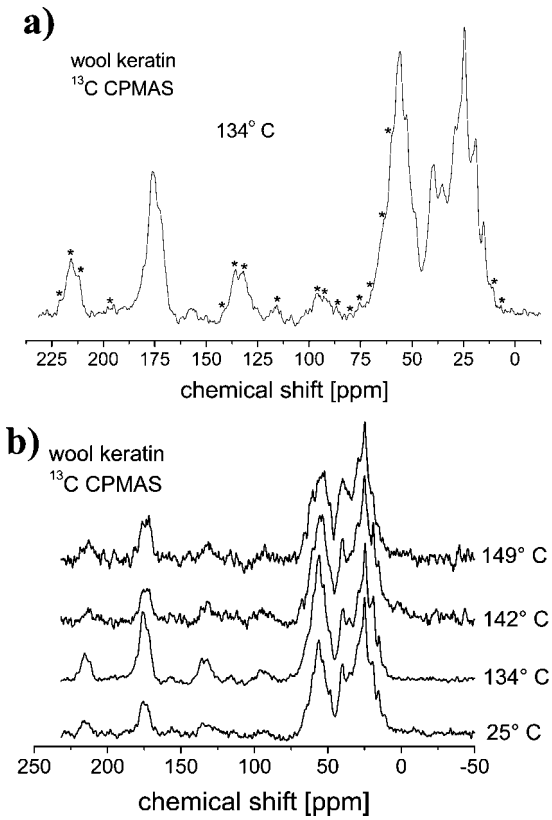

Figure 14. (a) ^{13}C CPMAS spectrum of keratin fiber at 134 °C where the spinning sidebands are marked by stars; (b) ^{13}C CPMAS spectra of hydrated wool keratin as a function of denaturation temperature.

put in evidence. It is evident that the interface mobility gradient is almost the same for the native hydrated wool sample and the sample denaturated at 160 °C. The largest gradient in the molecular mobility of about 11 kHz/nm is seen for the keratin proteins at the denaturation temperature of 149 °C. For all the other temperatures the gradient in mobility of the interfacial region is about 1 order of magnitude smaller than that at 149 °C.

4.8. ^{13}C CPMAS Spectra of Thermally Denaturated Wool Keratin. Cross-polarization (CP) MAS ^{13}C spectra of hydrated wool keratin denaturated at different temperatures are shown in Figure 14. These spectra are similar with those reported for α-keratin of equine hoof under hydrated conditions.[13] Many spinning-sidebands are present in the spectra because of (i) the large values of the ^{13}C chemical shielding anisotropy of carboxyl carbons and (ii) a relatively low spinning frequency of 5 kHz

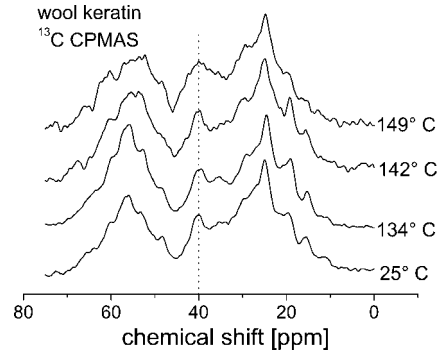

Figure 15. Enlarged version of the alkyl and α-carbon regions of the ^{13}C CPMAS spectra of Figure 14b for different denaturation temperatures. The dash line at 40 ppm marks the ^{13}C resonance of the cysteine engaged in the disulfide links.

(Figure 14a). The ^{13}C spectra show several distinct regions: (i) carbonyl region with a maximum at 173 ppm, (ii) a broader signal due to the α-carbons at 54 ppm, (iii) the peak at 40 ppm has contribution from β-carbon in leucine residues and the β-carbon in cross-linked cysteine residues, and (iv) a complex line shape in the 10−35 ppm region due to alkyl components of the side-chains (Figure 14b). The assignment was made following the ^{13}C isotropic chemical shifts for the common amino acid residues as reported in ref 13.

The ^{13}C CPMAS spectra from Figure 14b show that the line shape of the carbonyl signal has changed significantly with increasing of denaturation temperature. A larger degree of disorder of the intermediate filaments leads to a broadening of the resonances starting with the denaturation temperature of 142 °C. In the investigated thermal denaturation temperature range the amino acid residue composition does not change, and therefore the change in the carbonyl line shape must result from changes in conformation of the keratin.

In Figure 15 the enlarged region of the alkyl and α-carbon regions is shown. The peak at 40 ppm is related to β-carbon in cross-linked cysteine residues. These cysteine residues participate to the −S−S− disulfide links between neighboring keratin molecules. The intermolecular disulfide links between cysteine residues confer some degree of rigidity of the intermediate filaments in the amorphous matrix component of α-keratin. The broadening of the ^{13}C resonances at 40 ppm at the temperature of 149 °C over the denaturation temperature of 142 °C strongly suggest an increased heterogeneity of hydrated keratin due to the braking of a significant number of such −S−S− cross-links during the denaturation process. Additional nonfully resolved resonances in the region 32−40 ppm are due to glutamic acid, glutamine, and proline residues. Moreover, the spectral region at around 54 ppm is almost entirely associated with keratin random coil while the higher frequency region is associated with α-helical conformations.

4.9. Morphological Changes Induced by Thermal Denaturation as Seen by NMR Data. The model in Figure 16a gives a simplified schema of a microfibril with protofibrils showing the α-helical rods and the nonhelical terminal domains projecting into the interfilamentous space and linking with the matrix proteins through disulfide bonds. The terminal domains contain, besides cystine, glycine, threonine, valine, alanine, and serine, acidic sites as glutamic and aspartic acid. This way the electrostatic forces may well play a role for the stability of IFs in native fiber. This scaffolding structure at the IFs surface made by the side-chain interactions that anchor microfibrils to matrix (interface phase) assists the thermal stability and the primary control over the denaturation of helical structure of keratin

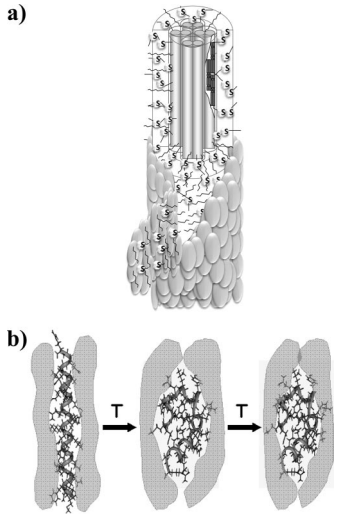

Figure 16. (a) Schematic representation of the intermediate filament imbedded in the keratin amorphous matrix. The waved lines show the disulfur bonds. (b) The frame representation of the sequence of keratin α-helix imbedded in the keratin amorphous matrix (gray areas) during the thermal denaturation. The keratin system at the ambient temperature is shown on the left frame. At the denaturation temperature of 142 °C the keratin α-helix folding is depicted (the frame in the middle). The reduction in the transverse average diameter of the rigid domain due to keratin reorganization is shown on the right frame.

materials when heated. It has a protective role and the capacity to participate in the formation of a solid interface.

The mechanism of thermal denaturation of keratins should therefore follow several steps (Figure 16b). Beyond a certain temperature (around 130 °C) the temperature rise leads to the breaking of scaffold structure of IFs. At that temperature the IFs are in a meta-stable state as shown by the left-hand frame of Figure 16b. The α-helix denaturates around at 80 °C in soluble proteins and it is only the interface that keeps it still organized. Once set free, the IFs (α-helices) denaturate. This involves a transition from a relatively compact ordered structure to a more flexible, disorganized, opened polypeptide chain (middle frame of Figure 16b). As the process of denaturation proceeds the protein molecules unfold (right-hand frame of Figure 16b) and the intern hydrophobic regions expose to the outside of the molecules. The hydrophobic groups in water tend to cluster, leading to associations of molecules.

5. Conclusions

Proton and ^{13}C NMR spectroscopy, double-quantum, and ^{1}H spin-diffusion were used for characterization of morphology, phase composition, segmental dynamics, and domain thicknesses for thermal denaturation investigation of hydrated wool keratin. For the first time the ^{1}H NMR spin-diffusion offers quantitative information about the side chain and segmental mobility heterogeneity of the interfacial region. The side chain motions play a very important role in the material properties of keratin. It may well be their degree of freedom which can dissipate stress during the mechanical deformation of keratin fibers.

These reported NMR results support the thermal denaturation pathway described above according to which concomitantly with the collapse of the scaffolds, the α-helices go from a relatively compact ordered structure to a more flexible, disorganized, open polypeptide chain. This is shown by an increase of the mobile phase at the expense of rigid- and interphase. Next, the protein molecules unfold and the intern hydrophobic regions expose to the outside of the molecules. The hydrophobic groups tend to cluster in the deuterated water, leading to associations of molecules and rebuilding the amount of rigid phase from the mobile phase. The interphase amount remains, however, at the same value, as no other reorganization occurs.

Acknowledgment. Support of this project by the Deutsche Forschungsgemeinschaft (DE 780/3-1 and PO 1333/1-1) is gratefully acknowledged. R.F. gratefully acknowledged the support of Romanian Ministry of Education and Research under Project PN II, ID-1102.

References and Notes

(1) Feughelman, M. *J. Appl. Polym. Sci.* **2002**, *83*, 489, and references therein.
(2) Wortmann, F.-J.; Popescu, C.; Sendelbach, G. *Biopolymers* **2007**, *83*, 630.
(3) Wortmann, F.-J.; Popescu, C.; Sendelbach, G. *Biopolymers* **2008**, *89*, 600.
(4) Miles, C.; Ghelashvili, M. *Biophys. J.* **1999**, *76*, 3243.
(5) Haly, A. R.; Snaith, J. W. *Text. Res. J.* **1967**, *37*, 898.
(6) Leroy, M.; Cao, J. *Biopolymer* **2005**, *77*, 38.
(7) Budrugeac, P.; Miu, L.; Bocu, V.; Wortmann, F.-J.; Popescu, C. *J. Thermal Anal. Calorim.* **2003**, *72*, 1057.
(8) Budrugeac, P.; Miu, L.; Bocu, V.; Wortmann, F.-J.; Popescu, C. *J. Thermal Anal. Calorim.* **2004**, *77*, 975.
(9) Popescu, C.; Budrugeac, P.; Wortmann, F.-J.; Miu, L.; Demco, D. E.; Baias, M. *Polym. Degrad. Stab.* **2008**, *93*, 976.
(10) Ernst R. R.; Bodenhausen G., Wokaun A., *Principles of Nuclear Magnetic Resonance in One and Two Dimensions*; Oxford Univ. Press: Oxford, 1990.
(11) Wüthrich K. *NMR of Proteins and Nucleic Acids*; John Wiley & Sons, Inc.: New York, 1986.
(12) Duer M. J., Ed. *Solid-State NMR: Theory and Applications*; Blackwell Science Ltd.: Oxford, 2001.
(13) Duer, M. J.; McDougal, N.; Murray, R. C. *Phys. Chem. Chem. Phys.* **2003**, *5*, 2894.
(14) Mack, J. W.; Torchia, D. A.; Steinert, P. M. *Biochemistry* **1988**, *27*, 5418. (a) Perich, J. W.; Johns, R. B.; Thompson, A. R. *Aust. J. Chem.,* **1995**, *48*, 1925.
(15) Yoshimizu, H.; Ando, I. *Macromolecules* **1990**, *23*, 2908.
(16) Nishikawa, N.; Horiguchi, Y.; Asakura, T.; Ando, I. *Polymer* **1999**, *40*, 2139.
(17) Nishikawa, N.; Tanizawa, Y.; Tanaka, S.; Horiguchi, Y.; Asakura, T. *Polymer* **1998**, *39*, 3835.
(18) Schmidt-Rohr, K.; Spiess, H. W., *Multidimensional Solid-State NMR and Polymers*; Academic Press: London, 1994.
(19) VanderHart, D. L.; McFadden, G. B. *Solid State Nucl. Magn. Reson.* **1996**, *7*, 45.
(20) Demco, D. E.; Johansson, A.; Tegenfeldt, J. *Solid State Nucl. Magn. Reson.* **1995**, *4*, 13.
(21) Buda, A.; Demco, D. E.; Bertmer, M.; Blümich, B.; Litvinov, V. M.; Penning, J.-P. *J. Phys. Chem. B* **2003**, *107*, 5357.
(22) Buda, A.; Demco, D. E.; Bertmer, M.; Blümich, B.; Litvinov, V. M.; Penning, J.-P. *Chem. Phys. Chem.* **2004**, *5*, 876.
(23) Wang, J. *J. Chem. Phys.* **1996**, *104*, 4850.
(24) Buda, A.; Demco, D. E.; Bertmer, M.; Blümich, B.; Reining, B.; Keul, H.; Höcker, H. *Solid State Nucl. Magn. Reson.* **2003**, *24*, 39.
(25) Crank J. *The Mathematics of Diffusion*; Clarendon Press: Oxford, 1975.
(26) Popescu, C.; Hoecker, H. *Chem. Soc. Rev.* **2007**, *36*, 1282, and references therein.
(27) Deutz, H.; Wortmann, F.-J. *J. Appl. Polym. Sci.* **1998**, *68*, 1991.
(28) Istrate, D.; Popescu, C.; Er Rafik, M.; Möller, M. *Biopolymer* **2008**, submitted.

JP8094616